A Histology-Based Model of Quantitative T1 Contrast for In-vivo Cortical Parcellation of High-Resolution 7 Tesla Brain MR Images

Juliane Dinse[1,2], Miriam Waehnert[1], Christine Lucas Tardif[1], Andreas Schäfer[1], Stefan Geyer[1], Robert Turner[1], and Pierre-Louis Bazin[1]

[1] Max Planck Institute for Human Cognitive and Brain Sciences, Leipzig, Germany
[2] Faculty of Computer Science, Otto-von-Guericke University, Magdeburg, Germany

Abstract. A conclusive mapping of myeloarchitecture (myelin patterns) onto the cortical sheet and, thus, a corresponding mapping to cytoarchitecture (cell configuration) does not exist today. In this paper we present a generative model which can predict, on the basis of known cytoarchitecture, myeloarchitecture in different primary and non-primary cortical areas, resulting in simulated in-vivo quantitative T1 maps. The predicted patterns can be used in brain parcellation. Our model is validated using a similarity distance metric which enables quantitative comparison of the results with empirical data measured using MRI. The work presented may provide new perspectives for this line of research, both in imaging and in modelling the relationship with myelo- and cytoarchitecture, thus leading the way towards in-vivo histology using MRI.

Keywords: myeloarchitecture, cytoarchitetcure, ultra-high resolution MRI, cortical parcellation.

1 Introduction

The human brain is a highly convoluted organ with many folds and fissures. Cortical activity and functional processing occur in a 2-4 mm thin sheet, typically consisting of six cellular layers. Over the 20^{th} century, cortical cartographers investigated the number, arrangement, and internal organisation of anatomically and functionally distinct areas of the cortex. Two major streams of research evolved: the disciplines of cytoarchitecture and myeloarchitecture. Cytoarchitecture deals with the cellular configuration within tissue. Brodmann pioneered these studies and produced the first qualitative and quantitative measures in layers in different cortical areas [1]. A decade later, von Economo and Koskinas published a full set of tables for 40 cortical areas, taking into consideration the absolute and relative values for different measures per layer. These include the thickness, the cell density as well as the cell size [2]. In contrast to cytoarchitecture, myeloarchitecture has been largely neglected. This discipline examines the cortical structures and anatomical features associated with the myelin sheaths of neuronal axons. Research in this field is incomplete, inconclusive [3] or even

K. Mori et al. (Eds.): MICCAI 2013, Part II, LNCS 8150, pp. 51–58, 2013.

contradictory. From classical histology, we know that cyto- and myeloarchitectonic images are projections of one and the same reality: the cortical architecture [4]. It should not be surprising, that there is a relation between the two fields. Hellwig [5] demonstrated in 14 cortical areas that a priori information of cytoarchitecture can be transformed into information regarding relative cortical myelin density. Only recently, neuroscientists found that cortical myelin provides MRI contrast, enabling segregation of primary areas based on cortical profiles running perpendicular through the depth of the cortex [6,7,8]. The first successful parcellations resulting in a classification of so-called Brodmann Areas (BA) have used cortical folding patterns [9], however with consistency only in primary areas.

In this paper we present a generative model which can predict, on the basis of known cytoarchitecture, in-vivo quantitative maps of T1 measured using MRI, to the extent that such maps represent myelin density. Our model parcellates the cortex based on purely intracortical features observable in ultra-high resolution structural MRI data, requiring accurate definition of profiles across the cortical thickness. This histology-based T1 model is validated in the motor-somatosensory region M1/S1 using a similarity distance metric, which enables comparison of the results with empirical data, and is extendable to additional cortical areas. The approach may provide novel insights regarding the correspondence of cyto- and myeloarchitectonic boundaries, and help to bridge the gap between macroanatomy and microanatomy, bringing MRI a step closer to in-vivo histology.

2 Methods

In order to predict myelin patterns of T1 from cytoarchitecture, we developed a two-step approach. The first step revisits the work of Hellwig [5], deriving myelin density profiles from cellular components forming patterns specific to different BAs (Fig. 1, top row). In the second step, to make these patterns relevant to MRI, we normalize the profiles into the scale of values of T1 (in seconds) found with 7 Tesla (T) MRI in brain tissue (Fig. 1, bottom row). This entails a regridding step that takes the MRI resolution and partial voluming effects into account. Finally, we model the variation of T1 values of these MR adjusted profiles in each BA, and build a probabilistic model with which we classify empirical profiles obtained from in-vivo MRI.

2.1 Generating Cortical Myelin Density Profile Shapes

Firstly, we obtain from von Economo and Koskinas [2] the relative thickness, mean cell size c_{size}, and mean cell density $c_{density}$ for each cortical layer within our regions of interest (ROI), here: BA 1, 2, 3b and 4 (Fig. 1 a). According to Hellwig [5], myeloarchitecture is predictable from cytoarchitecture by assuming that the quantity of myelin depends on cell size, following the sigmoidal function:

$$s(c_{size}) = 1/(1 + \exp(-r \cdot (c_{size} - l))) \quad (1)$$

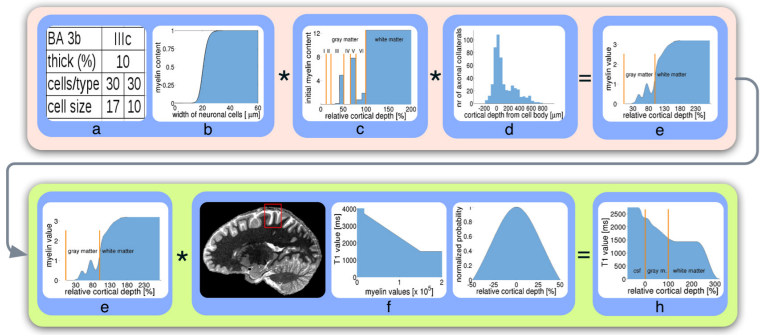

Fig. 1. The pipeline shows our two-step approach: the top row follows the work of Hellwig [5]. The second row transforms the myelin density profiles into generative profiles of the T1 intracortical contrast observable in MRI.

in which l describes the location of maximum contribution and r the rate of change (Fig. 1 b). Thus, we can obtain an estimate of myelin density (Fig. 1 c) for each layer c_{layer} as:

$$c_{layer} = c_{size} \cdot c_{density} \cdot s(c_{size}). \tag{2}$$

The horizontal pattern of myelinated fibers in the cortex originates mainly from axonal collaterals of pyramidal cells. To include these projections in our profile shapes, we convolve the myelin density estimates c_{layer} with a function a [10] (Fig. 1 d) describing the number of axonal collaterals at each cortical depth d:

$$m_{BA}(d) = \int_0^1 c_{layer}(x) \cdot a(d-x)\mathrm{d}x. \tag{3}$$

The profiles m_{BA} (Fig. 1 e) give a qualitative indicator of myelin concentration in the cortex and are comparable to myelin stained sections and myeloarchitecture described by Vogt [3].

2.2 Normalization to MR Intensities and Limiting Effects

Geyer et al. [7] demonstrated that quantitative T1 maps obtained with 7 Tesla (T) MRI reveal local differences of cortical structure reflecting the boundaries of functional areas. Glasser and Van Essen [8] showed that similar features could be observed at 3T, using another method of emphasizing T1 contrast. In order to apply the present model to such data, the convolved myelin density graph needs to be normalized into the scale of quantitative T1 maps, individually defined for each subject by the mean and standard deviation of T1 at the boundaries of white matter (WM)/gray matter (GM) and GM/cerebrospinal fluid (CSF). Besides inter-individual differences, further variability in the scale of T1 values originates from the comparatively coarse resolution available with in-vivo MRI

even at 7T, leading to partial voluming effects. These effects become more severe when neighboring tissues such as GM and CSF have a large difference in T1 values. Thus, profiles of the cortex have usually greater variance at the GM/CSF interface than at the WM/GM interface. In order to model myelin density profiles more realistically, we have to take account of this variability in the normalization step. First, we define an intensity scale $I_{BA} = [I_{BA}^{wm}, I_{BA}^{csf}]$ for each individual BA which is defined by the cortex average intensity μ_{gm} and standard deviation σ_{gm} at the WM/GM and CSF/GM interfaces as:

$$I_{BA}^{wm} = \mu_{wm,gm} - \hat{e}_{wm,BA}\ \sigma_{wm,gm} \quad \text{and} \quad I_{BA}^{csf} = \mu_{csf,gm} - \hat{e}_{csf,BA}\ \sigma_{csf,gm}. \tag{4}$$

The varying underlying myeloarchitectonic patterns in different areas result in differing cortical profiles within the spread of T1 times of the cortex (Fig. 1 f, left). $\hat{e}_{wm}$ and $\hat{e}_{csf}$ are the estimators of this variation which we found empirically. These estimates allow us to normalize the profiles given in $m_{BA}(d)$ into the T1 contrast of GM in given cortical depths d as:

$$T1_{BA}(d) = I_{BA}^{wm} + \frac{(I_{BA}^{csf} - I_{BA}^{wm})(m_{BA}(d) - min(m_{BA}(d)))}{max(m_{BA}(d)) - min(m_{BA}(d))} \tag{5}$$

in which $min()$ and $max()$ define the minimum and maximum of function $m_{BA}(d)$, respectively. Afterwards, we assign T1 values taken from [11] to WM and CSF outside the GM of the profile (Fig. 1 f, middle). At this point, our modelled T1 profiles are still continuous and resolution-free. To match the discrete limited MR resolution and to account for partial voluming at interfacing tissues, we convolved $T1_{BA}$ with a Lorentzian kernel (Fig. 1 f, right) to adjust resolution effects:

$$\tilde{T}1_{BA}(d) = \int_0^1 T1_{BA}(x)\ \frac{\sigma_{MR}}{((d-x) - \mu_{MR})^2 + \sigma_{MR}^2}\ \mathrm{d}x \tag{6}$$

in which μ_{MR} corresponds to the MR resolution used and σ_{MR} describes the overlapping ratio between MR resolution and the cortical thickness in individual BAs given in [2]. $\tilde{T}1_{BA}$ is now a defined function of myelin density in MR space and can be modelled from known cytoarchitecture in individual BAs (Fig. 1 h).

2.3 Probabilistic Modelling of Profiles

Given the limitations of MR, two questions remain: first, do individual empirical profiles derived from our data fit well into the model? Secondly, does this model actually allow segregation of different functional cortical areas in living subjects? In order to allow quantitative analysis, we need to estimate the expected variance of our modelled profiles. This variance also models uncertainties in the location of the profiles and is the dominant source of noise in our model. We defined σ_{BA}^{modMR} as the range of uncertainty by linearly interpolating empirical estimates of plausible deviations in individual Brodmann areas. Under the assumption that our T1 values, independently of their cortical depth, are normally distributed,

we can define the probability $P(p^{emp} \in BA)$ of a single profile p^{emp} to belong to a certain BA as an adaptation of a Gaussian process:

$$P(p^{emp} \in BA) \simeq \exp\left(\frac{1}{2\int_0^1 w_{BA}(x)\mathrm{d}x}\int_0^1 \frac{(p^{emp}(x) - p_{BA}^{modMR}(x))^2}{\sigma_{BA}^{modMR}(x)^2} w_{BA}(x)\mathrm{d}x\right) \quad (7)$$

We compare empirical profiles p^{emp} to MR adjusted profiles $p_{BA}^{modMR} \in \tilde{T1}_{BA}$ according to their cortical depth d. We added a weighting function w_{BA} to (7) as:

$$w_{BA}(d) = 1 - \exp\left(\frac{1}{2}\frac{(p^{ctx}(d) - p_{BA}^{mod}(d))^2}{\sigma^{ctx}(d)^2}\right). \quad (8)$$

In (8), the cortex average profile p^{ctx} is put into relation to the unsmoothed profile $p_{BA}^{mod} \in T1_{BA}$ in order to decrease the impact of partial voluming within the profiles at the boundaries with WM and CSF. To allow quantitative comparisons, we compute in all subjects the probability P for all single profiles p^{emp} of the whole cortex based on given modelled profiles. Distribution of probabilities in one given ROI vary due to different models. In plausible locations, probabilities are expected to be high and the distribution curve slanted towards 1, whereas in other regions the probabilities are expected to be lower and distributions slanted towards 0. We compute subject-wise in each ROI the mode of the distribution of the probabilities and the variance as Full-Width-Half-Maximum. This approach allows a quantitative individual and group-wise comparison of average probabilities $\bar{\mathrm{P}}$ between different BAs based on a given model.

3 Experiments

We scanned 10 human subjects on a 7T MR system with the MP2RAGE sequence [12,13] to obtain a whole-brain quantitative T1 map at $0.7\,mm$ isotropic resolution ($\mathrm{TI}_1/\mathrm{TI}_2$=900/2750 ms, TR=5 s, TE=2.45 ms) and maps of each hemisphere separately at $0.5\,mm$ isotropic resolution. The three maps were co-registered into a standard anatomical (Montreal Neurological Institute, MNI) reference space at $0.4\,mm$ isotropic resolution and fused to generate a whole-brain map from the two hemispheric $0.5\,mm$ maps. The cortex was extracted using in-house software based on the CRUISE algorithm [14]. The boundaries φ_{GW} between GM and WM and φ_{GC} between GM and CSF were used to estimate a set of N=20 level set surfaces $\{\varphi_d\}_{d=1,\ldots,N}$ based on a novel volume-preserving approach which parallels cortical layers in areas of curvature [15]. Orthogonal profile curves can be easily generated based on the level set representation. From the $0.5\,mm$ data we computed profiles covering the cortical depth to allow quantitative comparison between modelled and empirical profiles. Fig. 2 gives an impression of our data processing in detail. ROIs in the left hemispheric $0.5\,mm$ map have been defined and manually labeled guided by accepted macro-anatomical landmarks [16]. Our ROIs correspond to BA 1, 2, 3b and 4

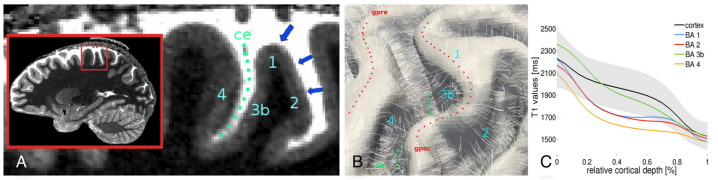

Fig. 2. MR data processing in detail: (A) 0.5 mm T1 maps with visible intracortical contrast (blue arrows) in BAs at the central sulcus (ce). (B) is the surface at WM/GM boundary with 3D profile curves at precentral (gpre) and postcentral gyrus (gpoc). (C) Mean empirical profiles derived from the data in ROIs.

and consist of 2500 up to 9500 voxels. Table 1 displays the empirically found estimates $\hat{e}_{wm}$ and $\hat{e}_{csf}$ and σ_{BA}^{modMR} at WM/GM and GM/CSF interfaces for the individual BA. Fig. 3 is highlighting all results for one subject. In the first row, the modelled (magenta, dashed) and MR adjusted (red, solid) profiles are illustrated in comparison to mean empirical profiles (blue, solid) derived from the data at given labels in the ROIs. The lighter bands represent the modelled and measured standard deviations. The final models correspond well to empirical profiles. In standard view, we demonstrate that probabilities computed in ROIs are always higher when model and respective BA are matching (Fig. 3, mid row). The last row in Fig. 3 gives a general impression of the distribution of the probabilities on the cortical surface. The focus is on our chosen ROIs. BA 4, 3b and 1 show particularly good results. The surfaces show inconsistent patterns when BA and model do not match which is noticable on the surfaces for BA 4 and 3b. Table 2 displays the quantitative comparison between modelled profiles in all ROIs on a group average and the single subject presented in Fig. 3. The variance is given in brackets. The diagonal describes the average probability $\bar{\mathrm{P}}$ of a given model in its corresponding location and anatomically neighboring areas are highlighted in yellow. In both tables the probabilities are very high in plausible locations on average and the variance remains small. If a model and BA are not matching, probabilities decrease and variance increases.

4 Conclusion

Following Hellwig [5], we established a generative histology-based model of quantitative T1 contrast, which assists observer-independent in-vivo cortical parcellation of high-resolution 7T brain MR images. For the first time, we have differentiated closely related cortical functional areas using solely quantitative

Table 1. The estimates $\hat{e}$ and σ_{BA}^{modMR} (in ms) for defining our modelled profiles

	$\hat{e}_{BA\,4}$	$\hat{e}_{BA\,3b}$	$\hat{e}_{BA\,1}$	$\hat{e}_{BA\,2}$	$\sigma_{BA\,4}^{modMR}$	$\sigma_{BA\,3b}^{modMR}$	$\sigma_{BA\,1}^{modMR}$	$\sigma_{BA\,2}^{modMR}$
WM	0.25	0.25	0.25	0.25	45	55	55	60
CSF	0.459	-0.444	0.053	0.130	170	170	170	140

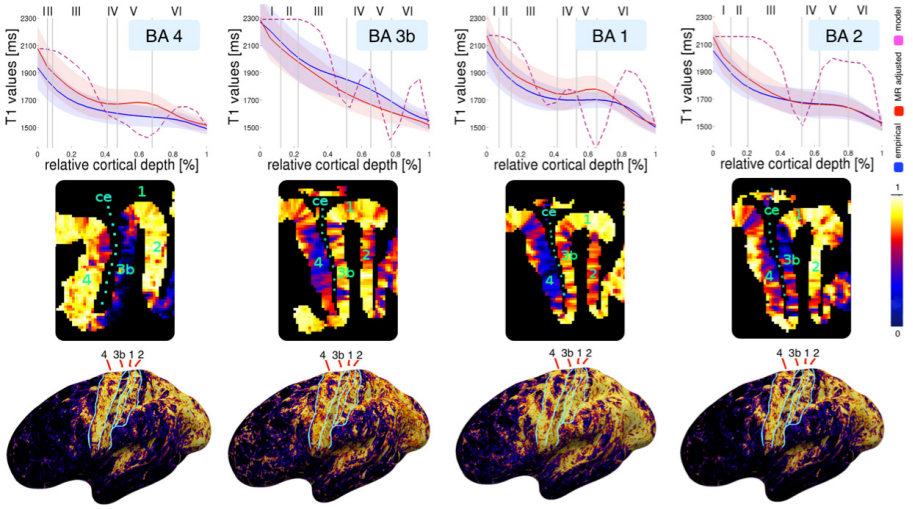

Fig. 3. Results of a single subject: the profiles (left) correspond well with the profiles derived from empirical data. Probabilities (middle row: standard view, bottom row: on the surface) are higher (coded yellow) in plausible locations.

Table 2. Quantitative results of $\bar{P}$ on group and single subject basis

	Labelled ROI (group average)				Labelled ROI (single subject)			
Modelled Profiles	BA 4	BA 3b	BA 1	BA 2	BA 4	BA 3b	BA 1	BA 2
BA 4	.750 (.466)	.671 (.328)	.693 (.438)	.726 (.356)	.87 (.55)	.00 (.02)	.83 (.31)	.86 (.36)
BA 3b	.593 (.511)	.888 (.261)	.698 (.471)	.648 (.474)	.71 (.77)	.87 (.26)	.77 (.45)	.64 (.55)
BA 1	.433 (.519)	.707 (.538)	.732 (.455)	.732 (.397)	.19 (.63)	.66 (.94)	.89 (.25)	.81 (.42)
BA 2	.626 (.517)	.691 (.302)	.726 (.460)	.699 (.440)	.68 (.88)	.00 (.01)	.80 (.31)	.83 (.45)

measurements of intra-cortical contrast. We have validated our model using real data, and have provided quantitative comparisons. Although the averaged global data still lacks some overall consistency, results on individual subjects can be much more accurate. Small motion and imaging artefacts may strongly affect these results, and methods for removing motion artifact, such as prospective motion correction, are likely to increase reproducibility. Another limitation of our model is the current resolution of $0.5\,mm$ constrained by the scan duration. Below a cortical thickness of $1.5\,mm$, the empirical profiles carry only a small amount of information compared with our modelled profiles. The approach presented offers completely new perspectives for this line of research, both in imaging and in modelling the relationship between myelo- and cytoarchitecture. In combination with these, our approach leads the way towards in-vivo histology, in the context of the increasing interest in new advanced methods in brain segmentation and cortical architectural studies.

References

1. Brodmann, K.: Vergleichende Lokalisationslehre der Großhirnrinde in ihren Prinzipien dargestellt auf Grund des Zellenbaues. JA Barth, Leipzig (1909)
2. Economo, C., Koskinas, G.N.: Die Cytoarchitektonik der Hirnrinde des Erwachsenen Menschen. Wien und Berlin (1925)
3. Vogt, C., Vogt, O.: Allgemeinere Ergebnisse unserer Hirnforschung. Erste Mitteilung. Ziele und Wege unserer Hirnforschung. J. Psychol. Neurol. 25 (1919)
4. Nieuwenhuys, R.: The myeloarchitectonic studies on the human cerebral cortex of the Vogt–Vogt school, and their significance for the interpretation of functional neuroimaging data. Brain. Struct. Funct. 218, 303–352 (2013)
5. Hellwig, B.: How the myelin picture of the human cerebral cortex can be computed from cytoarchitectural data. A bridge between von Economo and Vogt. J. Hirnforsch. 34, 387–402 (1993)
6. Wald, L., Fischl, B., Rosen, B.: High-Resolution and Microscopic Imaging at High Field. In: Ultra High Field Magnetic Resonance Imaging, pp. 343–371. Springer, New York (2006)
7. Geyer, S., Weiss, M., Reimann, K., Lohmann, G., Turner, R.: Microstructural Parcellation of the Human Cerebral Cortex–From Brodmann's Post-Mortem Map to in vivo Mapping with High-Field Magnetic Resonance Imaging. Front. Hum. Neurosci. 5 (2011)
8. Glasser, M.F., Van Essen, D.C.: Mapping Human Cortical Areas In Vivo Based on Myelin Content as Revealed by T1-and T2-Weighted MRI. J. Neurosci. 31, 11597 (2011)
9. Fischl, B., Rajendran, N., Busa, E., Augustinack, J., Hinds, O., Yeo, B.T., Mohlberg, H., Amunts, K., Zilles, K.: Cortical Folding Patterns and Predicting Cytoarchitecture. Cereb. Cortex. 18, 1973–1980 (2008)
10. Paldino, A.M.: A computerized study of axonal structure in the visual cortex. Syracuse University (1975)
11. Rooney, W.D., Johnson, G., Li, X., Cohen, E.R., Kim, S.G., Ugurbil, K., Springer, C.S.: Magnetic field and tissue dependencies of human brain longitudinal $^{1}H_2O$ relaxation in vivo. Magn. Reson. Med. 57, 308–318 (2007)
12. Marques, J.P., Kober, T., Krueger, G., van der Zwaag, W., Van de Moortele, P.F., Gruetter, R.: MP2RAGE, a self bias-field corrected sequence for improved segmentation and T1-mapping at high field. NeuroImage 49, 1271–1281 (2010)
13. Hurley, A.C., Al-Radaideh, A., Bai, L., Aickelin, U., Coxon, R., Glover, P., Gowland, P.A.: Tailored RF pulse for magnetization inversion at ultra-high field. Magn. Reson. Med. 63, 51–58 (2010)
14. Han, X., Pham, D.L., Tosun, D., Rettmann, M.E., Xu, C., Prince, J.L.: CRUISE: Cortical reconstruction using implicit surface evolution. NeuroImage 23, 997–1012 (2004)
15. Bok, S.T.: Der Einfluß der in den Furchen und Windungen auftretenden Krümmungen der Großhirnrinde auf die Rindenarchitektur. Arch. Neurol. Psychiatr. 121, 682–750 (1929)
16. Geyer, S., Schleicher, A., Zilles, K.: Areas 3a, 3b, and 1 of human primary somatosensory cortex: 1. Microstructural Organization and Interindividual Variability. NeuroImage 10, 63–83 (1999)